Liping Wang · Ga Zhang

Centrifuge model test study on pile reinforcement behavior of cohesive soil slopes under earthquake conditions

Abstract In this study, dynamic centrifuge model tests were conducted to investigate the dynamic response of cohesive soil slopes with the use of stabilizing piles during an earthquake. The behavior of the pile reinforcement was analyzed based on the obtained deformation over the entire slope through image-based measurement, and the behavior of the slope was compared to that of an unreinforced slope. The piles significantly increased the stability of the slope and reduced its deformation during an earthquake. The bending moment of the piles exhibited a nearly triangular distribution due to the earthquake. The acceleration response of the slope increased with increasing elevation, and the displacement accumulated apparently irreversibly over the course of the earthquake. The piles significantly affected the deformation of the slope in a certain area, the boundary of which was defined using a continuous surface. A strain analysis of the slope demonstrated that the piles had a significant effect on the reduction in the deformation of the slope in their vicinities, and this effect expanded upward along the slope and arrested the possible slip surface that would have occurred in an unreinforced slope. Several influencing factors were simulated in the tests, and observation of these factors demonstrated that the dynamic response of the pile-reinforced slope was affected by the pile spacing, pile location, slope gradient, and input earthquake to varying extent.

Keywords Slope · Cohesive soil · Pile · Soil–structure interaction · Earthquake · Centrifuge model test

Introduction

Landslides are one of the most severe geologic hazards in the world. The stabilizing pile has been an important development for supporting unstable slopes in recent decades (e.g., Rogers and Glendinning 1997; Anbarasu et al. 2010). Accordingly, many methods have been proposed for the proper design of pile-reinforced slopes (e.g., Ito and Matsui 1975; Poulos 1995). An adequate design method is dependent on the reasonable evaluation of an entire slope's stability level in considering the behavior and benefits of stabilizing piles. A few evaluation methods were proposed based on a diverse range of analysis schemes, such as the limit equilibrium method (e.g., Yamagami et al. 2000), limit analysis (e.g., Ausilio et al. 2001), the finite-element method (e.g., Cai and Ugai 2000), and other rigorous or simplified methods (e.g., Jeong et al. 2003). Understanding reinforcement behavior is critical to creating an effective evaluation method for pile-reinforced slopes.

The piles in a reinforced slope usually serve as a resistant member against slope deformation. A series of 1g model tests was used to investigate strip-footing behavior in a pile-stabilized sandy slope and showed that the piles significantly improved the bearing capacity of the footing (El Sawwaf 2005). Long-term monitoring data were employed to analyze the bending moments and displacements of the piles used to stabilize a railway embankment

(Smethurst and Powrie 2007). The stability of a large-scale slope reinforced using piles and other measures was studied using field monitoring (Kang et al. 2009). A uniform lateral translation was applied using shear boxes on the slope to evaluate the stabilizing effects of small diameter piles (Thompson and White 2006). A new approach was then described to evaluate the stability of pile-reinforced slopes. Martin and Chen (2005) used the FLAC3D program to analyze an embankment reinforced using piles subjected to a translational failure, demonstrating that the pile–soil relative stiffness had a significant effect on the failure mode of the piles. In addition, it was determined that an understanding of the pile–slope interaction can be accomplished by observing the response of the piles to lateral ground spreading, as investigated by several tests (e.g., Imamura et al. 2004; Brandenberg et al. 2005; Ashford et al. 2006).

The pile–soil interaction was systematically investigated by subjecting piles to lateral loads transferred to the slope. The pressure distribution of the piles and the deformation characteristics of the soil were studied under different conditions (e.g., Mezazigh and Levacher 1998; Zhang et al. 2004; Rosquoet et al. 2007). These investigations helped to understand the behavior of the pile–soil interaction in a pile-reinforced slope.

Centrifuge model tests play an important role in investigating the behavior and failure mechanisms of slopes because they can reproduce the gravity stress field and the gravity-related deformation process (e.g., Take et al. 2004). Such testing approach has been widely used for investigating the behavior of reinforced slopes with different reinforcement structures, such as geomembranes, geotextiles, and soil nails (e.g., Zornberg and Arriaga 2003; Thusyanthan et al. 2007; Wang et al. 2010), and has been shown to be an effective tool for studying the behavior of reinforced slopes. The deformation analysis was conducted in centrifuge model tests to obtain fundamental rules and failure mechanisms under different loading conditions (e.g., Take and Bolton 2001; Zornberg and Arriaga 2003; Viswanadham and Rajesh 2009; Wang et al. 2010, 2011).

Pile-reinforced slopes have not been systematically investigated under earthquake conditions, even though earthquakes are one of the important causes of landslides (Huang et al. 2012). Moreover, the way in which piles affect slope deformation and prevent failure has not yet been definitively understood. In this paper, dynamic centrifuge model tests were conducted to investigate the dynamic response of cohesive soil slopes using stabilizing piles during an earthquake. The pile-reinforced behavior of the slope under earthquake conditions was focused mainly on the deformation analysis that was obtained over the entire slope through image-based measurement and compared to the behavior of an unreinforced slope. Several influencing factors were considered in the tests, including the pile layout, slope gradient, and input earthquake wave.

Table 1 List of centrifuge model tests

Test ID	Type	Slope (V/H)	Pile location (cm)	Pile spacing (cm)	Wave
Unreinforced-0	Primary	2:1	–	–	Earthquake wave
Reinforced-0	Primary	2:1	$x=-5.4$	10 (7.1D)	Earthquake wave
Reinforced-1	Comparison	1.5:1	$x=-5.4$	10 (7.1D)	Earthquake wave
Reinforced-2	Comparison	2:1	$x=-10$	10 (7.1D)	Earthquake wave
Reinforced-3	Comparison	2:1	$x=-5.4$	6.7 (4.8D)	Earthquake wave
Reinforced-4	Comparison	2:1	$x=-5.4$	10 (7.1D)	Sine wave

D pile diameter, x x-axis coordinate

Device and measurement

The centrifuge model tests were conducted using the 50-g ton geotechnical centrifuge at Tsinghua University. The earthquake was simulated with a specially manufactured shake table for this centrifuge, which can generate arbitrary horizontal earthquake waves with a maximum acceleration of 20g via a complex hydraulic pressure servo-system.

The aluminum alloy model container for the tests was 50 cm long, 20 cm wide, and 35 cm high. A transparent Lucite window was installed on one side of the container, through which the deformation process of the soil could be observed and recorded.

An image-capture and displacement measurement system was used to record images of the slope at a maximum rate of 48 frames/s during the centrifuge model tests (Zhang et al. 2009). An image correlation analysis algorithm was used to conduct a subpixel measurement of the displacement vectors of an arbitrary point in the soil without disturbing the soil (Zhang et al. 2006). This algorithm matched the gray scale pattern of a subregion with centroid as the measurement point between adjacent images using correlation analysis and determined the displacement of the measurement point according to the corresponding position in different images. It should be noted that the algorithm required to visualize a region with a random gray level distribution of the soil. Thus, the history of measurement point was obtained according to the capture times of processed images. The measurement accuracy can reach up to 0.02 mm at the model dimensions according to the resolution of captured images and calibration results in previous studies (Zhang et al. 2009).

Dytran-3035B accelerometers, with a range and accuracy of 50 g and 1 %, respectively, were buried in the slope to measure the acceleration response during the tests. Strain gauges were attached to the piles to measure their strain response. These transducers were linked to the automatic data acquisition system to obtain real-time records.

Test description

Schemes

Table 1 lists the centrifuge model tests conducted in this study. The primary centrifuge model tests were conducted on pile-reinforced and unreinforced slopes. The measured results, based on the model dimensions, were compared to investigate the behavior of the reinforced slopes. In this paper, the focus of influencing factors was placed on the pile layout and slope gradient, and the physical parameters of the soil, such as density and water content, were fixed in the centrifuge model tests. Some comparative centrifuge model tests were conducted to discuss the effectiveness of the knowledge gained and the influencing factors by altering slope gradient, pile spacing, pile location, and the input earthquake wave.

The earthquake was applied on the model slope at the centrifugal acceleration of 40g. The sizes of the slope and the pile as well as the measured results, which were presented based on the model dimension in this paper, can be converted to the prototype dimensions according to the similarity criterion of the centrifuge model tests (Table 2).
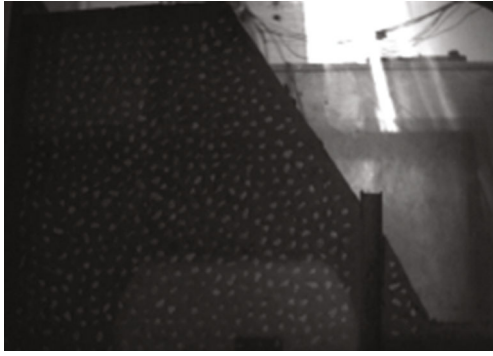
Models

Figures 1 and 2 show photographic and schematic views of the pile-reinforced model slope used for the primary test. The geometry of the unreinforced slope was identical to that of the pile-reinforced model. The soil was retrieved from the foundation of a building in Beijing, China. The plastic limit and liquid limit of the soil were 15.5 and 33.5 %, respectively. The soil was compacted into the container in 6-cm layers with a dry density of 1.4 g/cm³. The water content was maintained as 18 %, close to the optimum water content of the soil, with a degree of saturation of 55 %. The slope for the tests was obtained by removing redundant soil. In accordance with the container size, the slope was 2:1 (vertical/horizontal) and 28 cm in height that was equivalent to 11.2 m in the prototype dimension at a centrifugal acceleration of 40g (Fig. 2). It should be noted that the gradient of the slope, together with the dry density and water content of the soil, was comprehensively determined to realize a landslide of the unreinforced slope according to a few trial tests. Thus, the reinforcement mechanism can be investigated through comparison of responses between the reinforced and unreinforced slopes. The slope gradient was changed to 1.5:1 in a comparison test.

A 5-cm-high soil layer under the slope was included to diminish the influence of the bottom container plate on the deformation of the

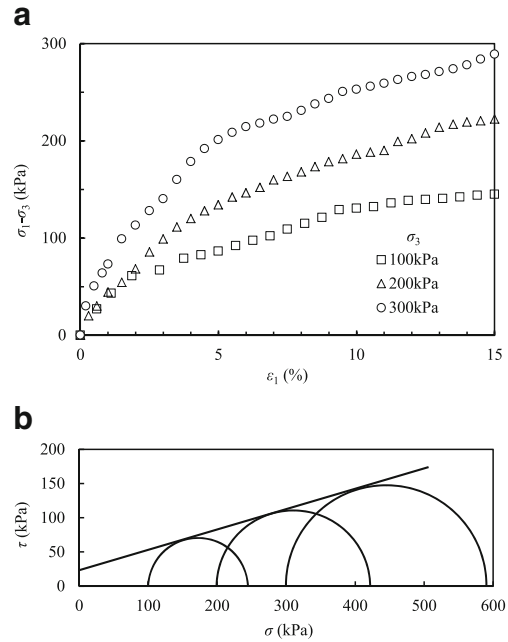**Table 2** Similarity criterion for centrifuge model tests

Centrifugal acceleration (g)	Strain	Stress	Length	Dynamic acceleration	Time	Displacement	Bending moment
n	1	1	n	$1/n$	n	n	n^3

Fig. 1 Photograph of the model of reinforced slope in Reinforced-0 test

Fig. 3 Drained triaxial test results of the soil. σ_1 maximum principal stress, σ_3 minimum principal stress, σ normal stress, τ shear stress, ε_1 axial strain. **a** Stress–strain relationship; **b** shear envelope and Mohr circle

slope. Silicone oil was painted on the sides of the container to decrease the friction between the slope and the container. Close examination results of the slope preliminarily indicated the effectiveness of these measures. For example, the slip surface of the unreinforced slope and the settlement at the top of the slopes exhibited approximately uniform distribution in direction perpendicular to the lateral side of the model.

It should be noted that partially saturated soil was used in the tests to avoid significant pore pressure in the slope due to earthquake that occurred in saturated soil. Thus, the research can focus on the pile influence on the response of the slope. Figure 3 shows the drained triaxial test results of the soil used for the centrifuge model tests, with a dry density of 1.4 g/cm³ and a water content of 18 %. A low loading rate was used in the triaxial tests after the soil was adequately consolidated

to a confining pressure, to assure that the pore water pressure and pore air pressure dissipated entirely during the tests. The deviation stress was discovered to increase as the axial strain increased and the rate of increase was significantly affected by the confining pressure (Fig. 3a). There was no peak in the deviator stress curve, which may be due to the normal consolidation state of the soil in the triaxial tests. The density of the soil was a bit small, and thus, the soil experienced a significant compression during the consolidation with application of a confining pressure. The deviator stress at the axial strain of 15 % was selected for the determination of strength parameters. The strength of the soil was described using the Mohr–Coulomb criterion, and the parameters were determined according to the triaxial tests with 22 kPa in cohesion and 17° in internal frictional angle (Fig. 3b).

A hollow square pipe made of steel with an elastic modulus of 210 GPa was used to simulate the stabilizing pile of the reinforced slope. The square section was selected for the piles for convenience in the attached strain gauges and analysis of pile–soil displacement. It is believed that the circular section and square section can reach similar rules for the response of the slope and pile. The side length of the pipe D was 1.4 cm with a wall thickness of approximate 1.5 mm. The pile was stiff enough to allow its deflection to be ignored in comparison to the neighboring soil. This setup was equivalent to a prototype pile with a side length of 0.56 m at a centrifugal acceleration of 40g. The piles were arranged in a single row with spacing of 10 cm (7.1D) and located in the lower part of the slope, 5.4 cm from the slope toe, for the primary test. The pile spacing was reduced to 4.8D, and the pile location was moved to the upper part of the slope in the comparative tests (Table 1). Half-section piles were used at both container ends to approximate the plane strain condition (Fig. 2b). The half-section pile was obtained by cutting a full pile in half and its width became 0.7 cm with the wall thickness maintained (Fig. 2b). In all tests, the piles were inserted in the slope to the bottom of the container without any special fixing.
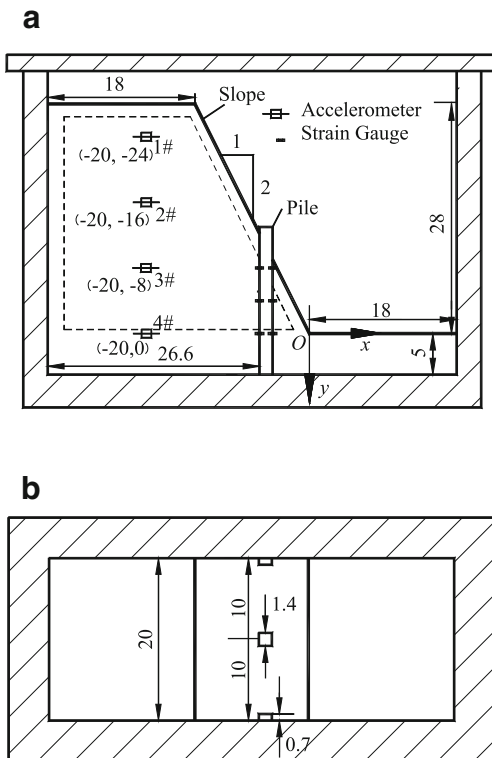
Fig. 2 Schematic view of the model of reinforced slope in Reinforced-0 test (unit: centimeter). **a** Elevation view; **b** vertical view

Figure 2 shows the main deformation zone used for image-based displacement measurements within a dashed line. White terrazzo particles were embedded in the lateral side of the slope as required by the image-based displacement measurement system (Fig. 1). Cartesian coordinates were established, with the slope toe as the origin, specifying positive as downward in the vertical direction (y-axis) and to the right in the horizontal direction (x-axis) (Fig. 2).

A series of accelerometers were buried in the soil to measure the acceleration response at different elevations during the earthquake (Fig. 2a). Four pairs of strain gauges were attached to the outer wall of the middle pile to measure strain along the shaft (Fig. 2a).

Procedures

The model slope was installed on the shake table of the centrifuge, and the centrifugal acceleration was gradually increased to 40g and then maintained for the duration of the test. After the deformation of the slope became stable at 40g level, a simulated earthquake wave was applied to the bottom of the container. This wave was obtained on the basis of the Park field earthquake, which lasted 1 s, with a maximum acceleration of 8.25g in the model dimension (Fig. 4), equivalent to 0.206g in the prototype dimension at a centrifugal acceleration of 40g. The shake simulated on the comparative model was a sine wave with an amplitude of 4.4g, equivalent to 0.11g in the prototype dimension, a period of 0.01 s, and duration of 7 s. The comparison of the two input waves indicated that the sine wave had significantly more energy than the simulated earthquake wave.

Dynamic response observation

Figure 5 shows the photograph of the unreinforced slope after earthquake. A distinct landslide occurred in the unreinforced slope during the earthquake and the slip surface was marked with curves in Fig. 5. Figure 6 shows the post-earthquake vertical displacement contours of the pile-reinforced and unreinforced slopes in the primary tests. It should be noted that the borders of the displacement contours were designated as dashed lines in Fig. 2 and not the actual slope borders. The vertical displacement was observed to increase with increasing elevation. Except for the practical slip surface, a potential slip surface can be derived according to the contour lines (Fig. 6a) and outlined with a dashed line in Fig. 5. However, the reinforced slope exhibited residual deformation as a result of the earthquake, and landslide was avoided (Fig. 6b). The horizontal displacement exhibited similar features with the vertical displacement and therefore was not presented here. Compared with the unreinforced slope, the stability level of the reinforced slope was greatly increased, with significant reduction in the post-earthquake deformation, which can be attributed to the effect of the piles.
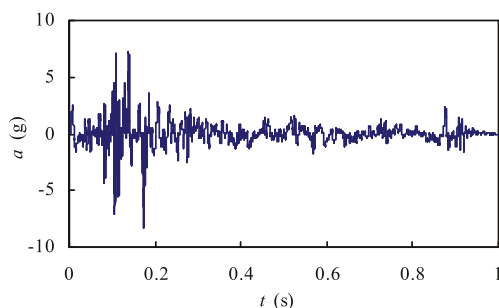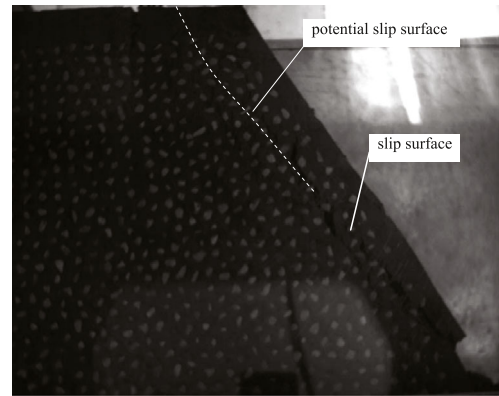

Fig. 5 Photograph of the unreinforced slope after earthquake

Figure 7 shows the seismic response of several points at the accelerometer locations in the pile-reinforced slope in the primary test. The horizontal displacement of the slope was presented to be relative to the
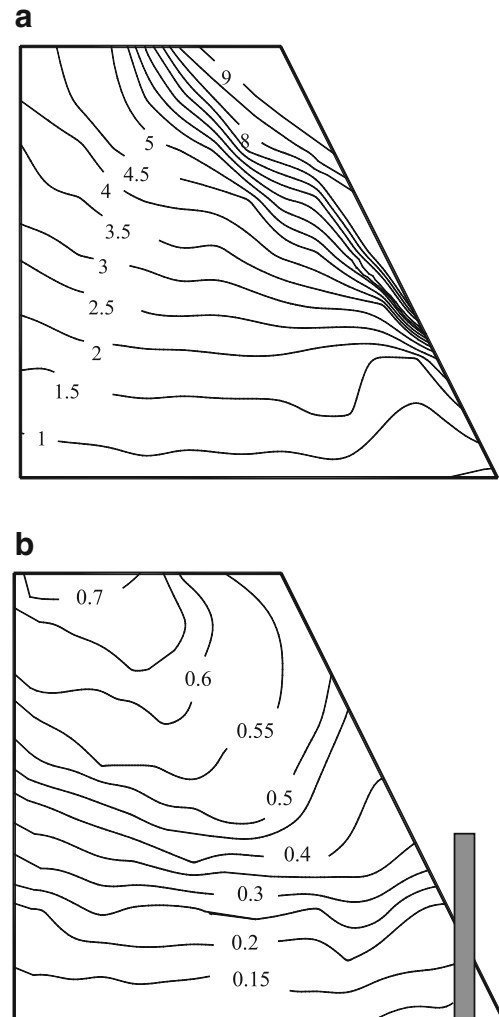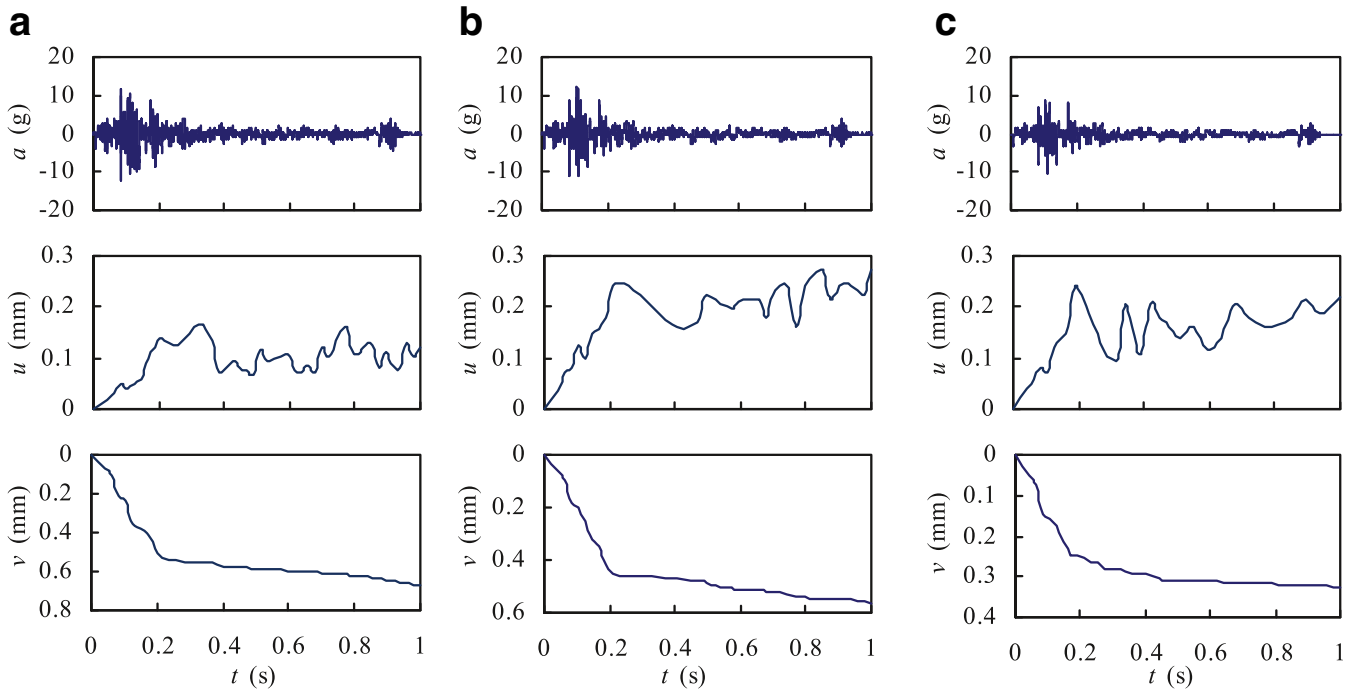

a

b

Fig. 6 Contour lines of the post-earthquake vertical displacement of slopes (unit: mm). **a** Unreinforced-0 test; **b** Reinforced-0 test

Fig. 4 Seismic wave input. t time, a acceleration

Fig. 7 Seismic response of typical points on a reinforced slope in Reinforced-0 test. *a* acceleration, *u* horizontal displacement, *v* vertical displacement, *t* time. **a** 1#; **b** 2#; **c** 3#

container. High-frequency displacement response waves were filtered, owing to the frame-rate limit of the capture images (48 frames/s) and measurement accuracy (0.02 mm), which prevented a few minor displacements from being captured. It should be noted that the dynamic response at the 4# accelerometer location was not presented because it was located in the soil foundation and used to verify the input wave.

The peak acceleration and peak vertical displacement both increased with increasing elevation (Fig. 7). During shaking, the horizontal displacement fluctuated in magnitude, with a tendency to accumulate in the direction pointing to the outside of the slope, and the vertical displacement monotonically increased. This demonstrated that the earthquake induced irreversible deformation of the slope. The irreversible deformation increased rapidly in the early period of the earthquake, accompanied by remarkable input acceleration, and the rate of increase lowered when the input wave faded. In other words, the rate of increase of deformation depended on the magnitude of the input shaking acceleration. Similar characteristics in dynamic response of the slope were obtained in other centrifuge model tests.

The maximum post-earthquake horizontal displacement was selected as an index to examine the influencing factors on the earthquake-induced deformation of the slope during centrifuge model tests (Fig. 8). It can be observed that the deformation of the slope decreased if the pile spacing (from 7.1*D* to 4.8*D*) or the slope gradient (from 2:1 to 1.5:1) was reduced, but it increased if the pile was moved from the lower part to the upper part of the slope or the sine wave was substituted for the earthquake simulation as the input wave.
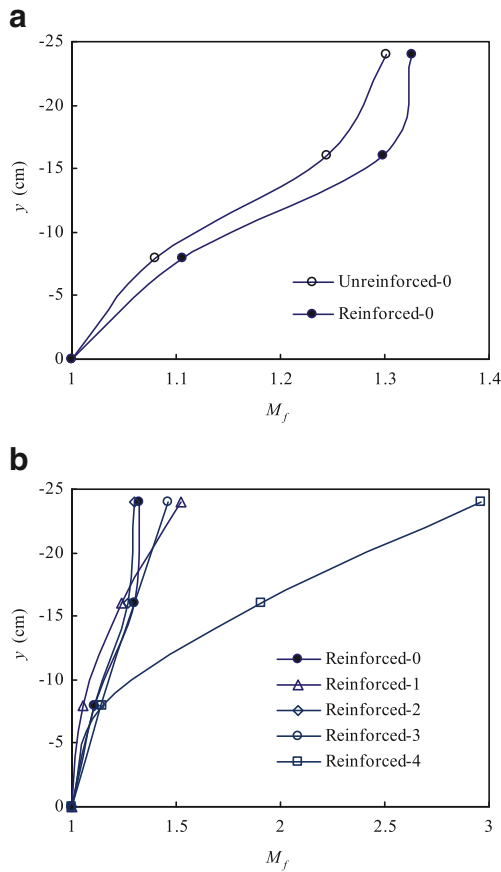
The amplification factors at the accelerometer locations were obtained using the acceleration histories (Fig. 9). The factors gradually increased with increasing elevation for all reinforced and unreinforced slopes. The reinforced slope exhibited slightly larger amplification factors than the unreinforced slope (Fig. 9a). The reason can be attributed to the influence of piles on the dynamic behavior of the

slope. The dynamic response of the slope was affected by the pile layout and slope gradient, which changed the dynamic behavior of the slope such as the natural frequency of the slope. The amplification factor increased significantly when the sine wave was substituted for the simulated earthquake wave (Fig. 9b). It can be concluded that the amplification factor was dependent both on frequency components of input motion and dynamic behavior of the slope.

The bending moment of the pile was derived according to the elastic mechanics theory using the measured strain, defined as positive in the clockwise direction. The histories of the bending moment exhibited an equivalent change with the input seismic wave and reached their maximum values when the input acceleration peaked. Figure 10 shows the post-earthquake maximum bending moments
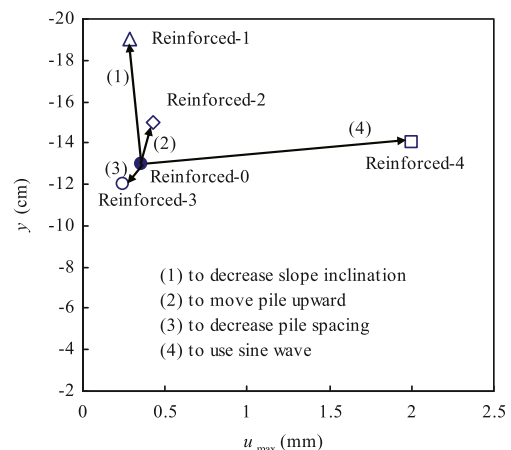
Fig. 8 Maximum post-earthquake horizontal displacements of slopes and their vertical coordinates. u_{max} maximum horizontal displacement
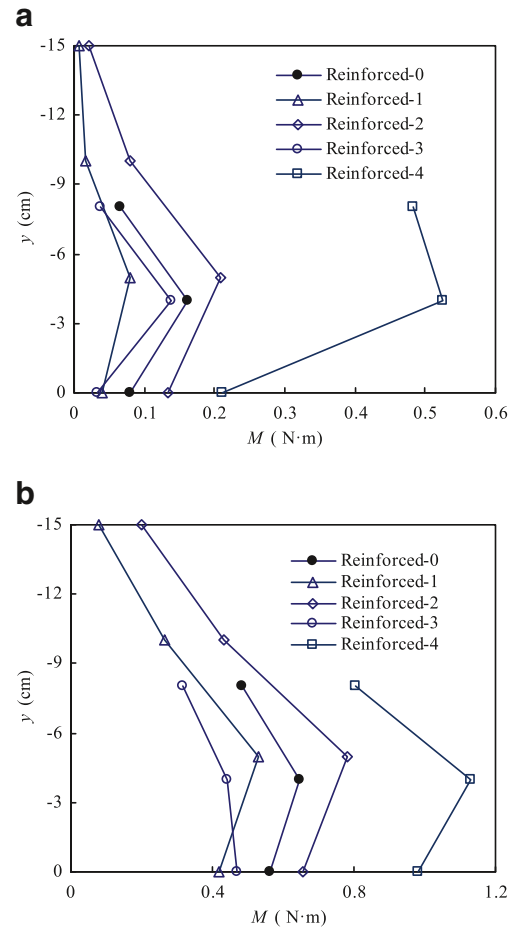
Fig. 9 a, b Distribution of amplification factors of acceleration in slopes in different tests. M_f amplification factor of acceleration

Fig. 10 Earthquake-induced bending moment distribution of piles in different tests. M bending moment. **a** Post-earthquake moment; **b** maximum moment

along the pile in different tests. It can be observed that the bending moment exhibited a nearly triangular distribution, peaking at the middle and lower parts of the pile.

The maximum and post-earthquake bending moments of the piles were influenced by the pile layout, the slope gradient, and the input earthquake wave through the centrifuge model tests (Fig. 10). The bending moment of the pile decreased if the pile spacing was reduced from $7.1D$ to $4.8D$ but increased if the pile location was moved from the lower part to the upper part of the slope. However, the bending moment of the pile significantly increased if the sine wave was used instead of the simulated earthquake but decreased if the slope gradient was reduced from 2:1 to 1.5:1. Similar behavior due to the influencing factors was demonstrated in the maximum horizontal displacement of the slope, implying that the bending moment of the pile had a close relationship with the deformation of the slope. For example, the earthquake induced larger deformation in the steeper slope, which resulted in more significant pile–soil interaction and larger bending moment of the pile. These results should be taken into consideration in the design of such piles.

The pile–soil interaction was preliminarily examined using pile–soil displacement that was obtained using image-based measurement. Figure 11 shows the post-earthquake horizontal displacements of a series of points in vertical lines in the reinforced slope in primary test, 1 cm away from the piles. The piles, significantly stiffer than the neighboring soil, exhibited a nearly linear horizontal displacement

distribution. The displacement of the pile was located between those of the soil on both sides, consistent with the continuity. The horizontal displacements of the pile and soil were both small near the pile end; thus, the pile–soil displacement was small. The pile–soil displacement was also small near the pile top. The pile–soil displacement exhibited its maximum near the middle of the piles on both sides (Fig. 11); this
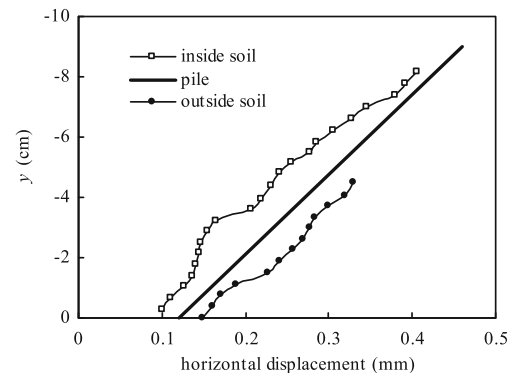
Fig. 11 Post-earthquake horizontal displacements of the pile and neighboring soil in the primary test

implied that there was a significant pile–soil interaction. The earth pressure on the pile was inferred to be dependent on the pile–soil displacement according to the understanding of the stress deformation behavior of the soil. Therefore, a nearly triangular distribution of earth pressure, with maximum near the middle of the pile, was estimated according to the distribution of pile–soil displacement in the test.

Pile influence behavior analysis

Displacement-based analysis

The deformation analysis of the pile-reinforced slope was based mainly on the displacement distribution of the lateral side of the slope in primary tests, during which the piles had the largest effect on the deformation of the slope. It is believed that the soil across the open space between the piles can be retained by soil-arching action, which was preliminarily confirmed by the test observation that the free surface of the slope exhibited negligible evagination between piles. Irreversible deformation of the slope induced by the earthquake application was observed (Figs. 6 and 7). As the piles are usually considered to be subjected to lateral forces by the horizontal movements of the surrounding soil, the distribution of post-earthquake horizontal displacement of the soil at a horizontal line was examined to investigate the influence of piles on the earthquake-induced deformation of the slope. Samples from five elevations were used to compare results from the reinforced and unreinforced slopes in the primary tests, covering the slope from top to bottom (Fig. 12). It should be noted that the displacements of the unreinforced and reinforced slopes were indicated using different axis scales, on the left and right sides of the figure.

A close examination of the displacement distribution of the soil at a horizontal line, $y=-3.2$ cm, showed a significant difference between the reinforced and unreinforced slopes (Fig. 12e). An inflection in the curve occurred near the pile ($x=-10$ cm) in the pile-reinforced slope. On the left side of the inflection, the horizontal displacement increased significantly from the inner slope area to the piles, whereas this rate of increase became fairly small on the right side. In addition, the horizontal displacement increased from the inner slope at an approximate constant rate in the unreinforced slope near the corresponding location of the piles in the reinforced slope. It can be concluded that the piles had a visible effect on the displacement distribution of the slope at a certain area near the piles, and this inflection can be regarded as a boundary point where the piles began affecting the deformation significantly.

The inflections can be found in the displacement distribution curves of the reinforced slope at all sampled elevations (Fig. 12). A continuous surface was obtained by connecting these inflections using a curve, as shown in Fig. 12 by the dotted line. This surface, denoted as the *W-surface* in this paper, indicates the boundary of the area where the piles significantly affected the deformation of the slope. The horizontal displacement of the pile-reinforced slope exhibited different distributions on the inner and outer sides of the W-surface. Thus, the W-surface was an important index for describing the pile-influenced behavior of the slope. The W-surface of the slopes was determined according to a series of distributions of post-earthquake horizontal displacement at
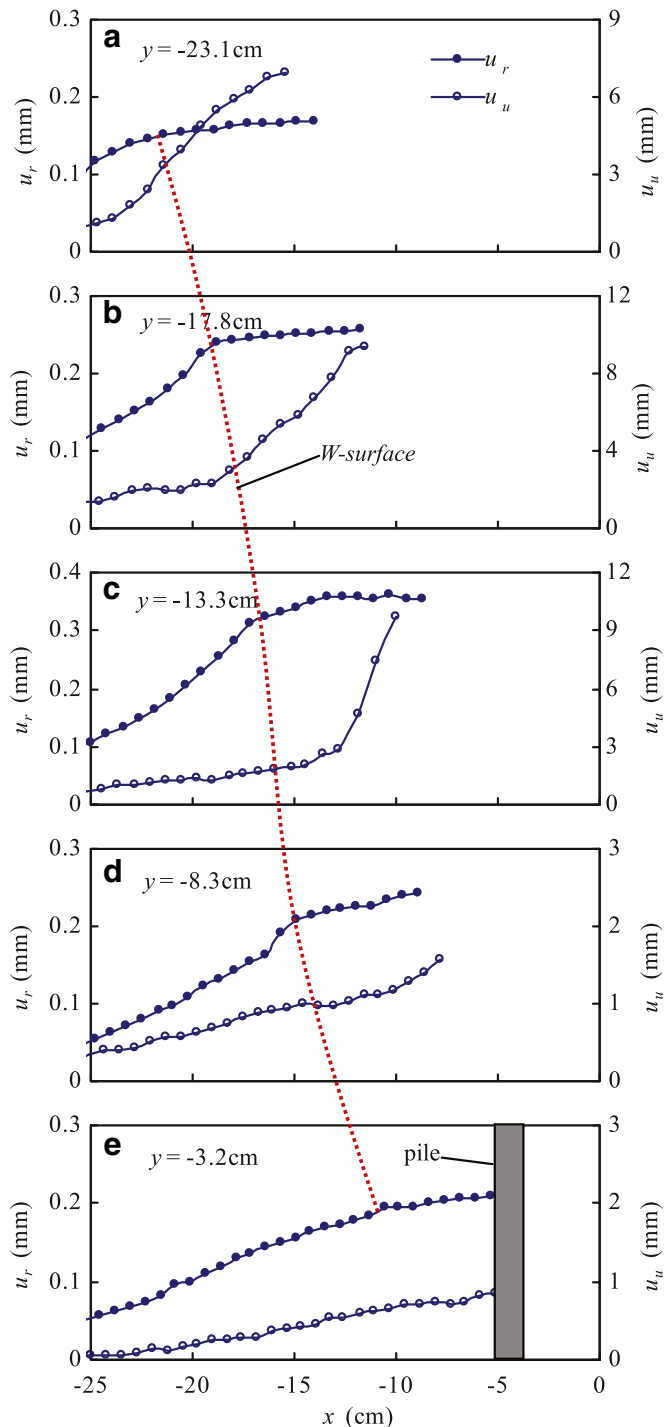
Fig. 12 a–e Post-earthquake horizontal displacement distributions of Reinforced-0 and Unreinforced-0 tests. u_r horizontal displacement of reinforced slope, u_u horizontal displacement of unreinforced slope

different elevations of the slope. In other words, the inflection of each distribution curve was marked, and the W-surface was obtained by connecting these inflections using a smooth curve.

According to the results given by the W-surface and the piles, the reinforced slope was divided into three zones on the inner side of the

pile: A, B, and C (Fig. 13). The slip surface of the unreinforced slope, including the potential surface, was also outlined in the figure for comparison. The deformation behavior exhibited different features in different zones. Zone A is the area at the inner side of the W-surface, far from the piles. Thus, the piles had a small effect on the deformation of this zone. In other words, the horizontal displacement of the reinforced slope showed a similar distribution to that of the unreinforced slope. Zone B is above the piles and has a free surface. The variation of deformation of the slope was small in this zone due to the restriction of the piles. Zone C is at the outside of the W-surface and is in direct contact with the piles. The piles significantly reduced the horizontal displacement of the soil in this zone, and the displacement distribution showed a flat curve. The soil on the outer side of the pile should support the piles during the earthquake.

The understanding derived from this analysis was deemed qualitatively suitable for the different pile-reinforced slopes in the centrifuge model tests in this paper, even though the deformation of the individual slopes was quantitatively affected by different factors. The W-surface, an important indicator used to characterize the reinforcement behavior of the slope, was determined using displacement distributions corresponding to different factors (Fig. 14). This surface could be described using a similar format, though its position and curvature were affected by different factors to various extent. For example, the W-surface moved into the slope if the pile was moved from the lower part to the upper part of the slope. Decreasing the pile spacing induced a slight movement of the W-surface into the slope in a similar manner. Compared with the gradient, the pile layout influenced the W-surface more significantly.

Strain-based analysis

Measurement of the strain of soil elements of the slope was introduced to analyze the pile reinforcement behavior of the slope. This strain was determined directly by a common finite-element method, as follows:

$$\{\varepsilon\} = [\mathbf{B}]\{\delta\}^{e} \tag{1}$$
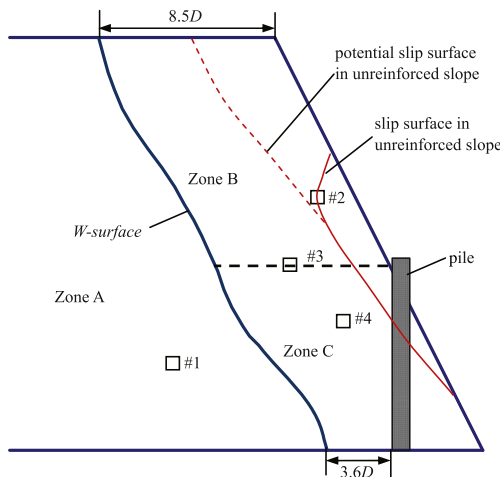
Fig. 13 Division of slope into zones representing different displacement behaviors in Reinforced-0 test. *D* side length of pile
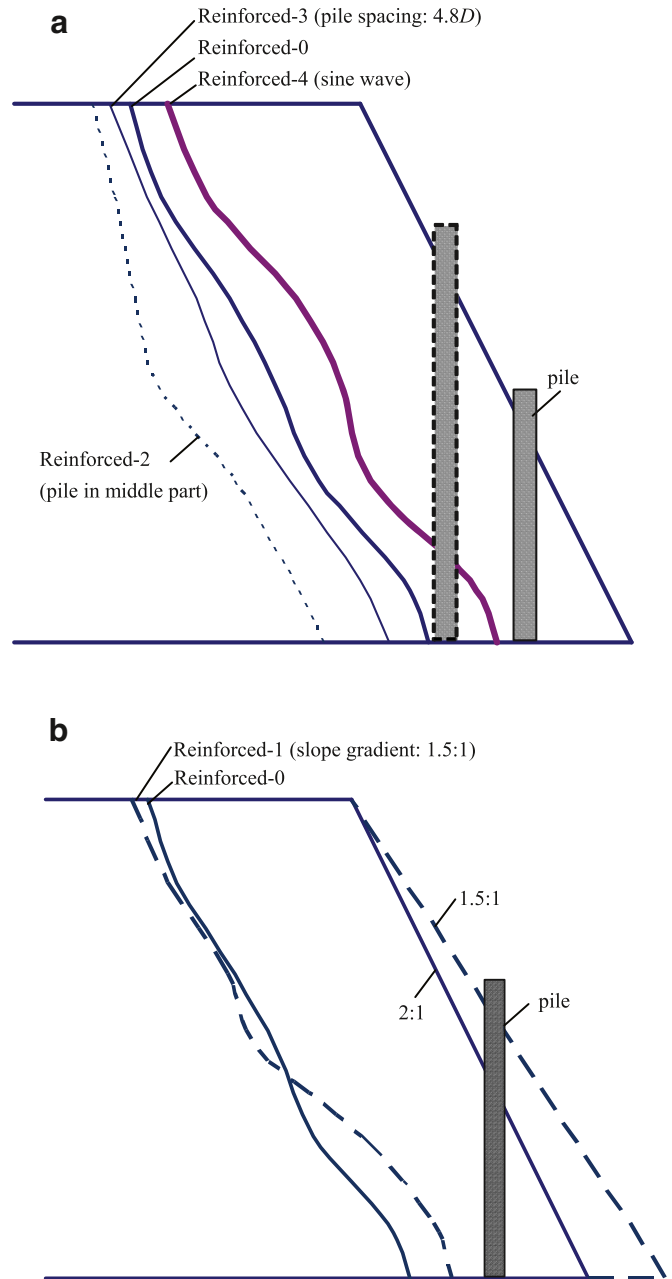
Fig. 14 a, b W-surfaces of the slope in different tests

where $\{\varepsilon\}$ is the strain vector of the element, and $\{\delta\}^{e}$ is the displacement vector of the nodes of the element. The transform matrix, $[\mathbf{B}]$, is widely known for the four-node isoparametric element (Gallagher 1974). In a departure from finite-element analysis, the displacement vector of the nodes, $\{\delta\}^{e}$, was directly obtained using the image measurement system. A 1-cm-long square element was used for the strain analysis. The strain at the center was assumed to be the strain of this element. All strain components, such as normal strain and shear strain at an arbitrary direction of the element, were easily derived from this measurement.

Figure 15 shows the strain histories of four typical elements on the three zones of the reinforced slope in Fig. 13, in comparison with the corresponding elements in the unreinforced slope. It
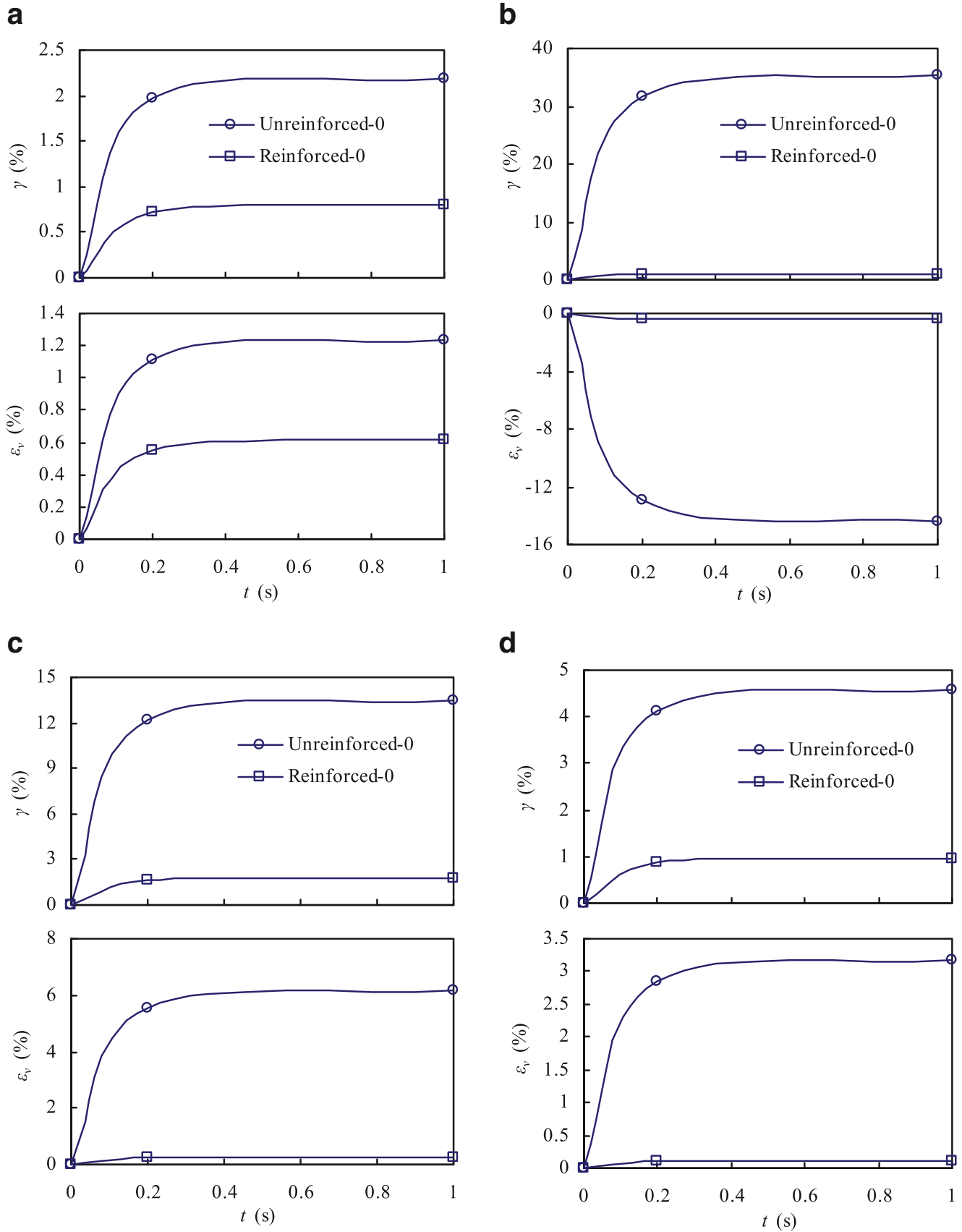
Fig. 15 Strain history of typical elements (location indicated in Fig. 13) during earthquake in the primary tests. γ slope direction shear strain, ε_v volumetric strain, t time. **a** Element #1; **b** element #2; **c** element #3; **d** element #4

should be noted that the slope direction shear strain was used in this study because the observation showed that the slip surface of the unreinforced slope was nearly parallel to the slope surface (Fig. 5). The compression volumetric strain was defined as positive.

In zone A, far from the piles, the compression and shear strain were both relatively small in the reinforced and unreinforced slopes (Fig. 15a). In zone B, the shear strain of element #2 in the unreinforced slope increased rapidly in the early period of the earthquake (Fig. 15b) and reached a large value when the landslide occurred across this element. In addition, the volumetric strain was dilative, different from the compressive volumetric strain of typical elements in other zones, because the dilative horizontal strain was fairly larger than the compressive vertical strain in the magnitude there. However, the shear strain increased at a smaller rate and reached a lower level far from failure when piles were used. In other words, the piles confined the shear deformation of the slope in this zone so that the shear strain was noticeably decreased. As a result, the piles arrested the formation of a slip surface and reduced the volumetric strain of zone B accordingly. The volumetric strain of element #4 in zone C, close to the piles, increased rapidly in the early period of the earthquake for both the reinforced and unreinforced slopes and tended to stabilize when the input seismic wave began to weaken (Fig. 15d). The volumetric strain and shear strain in the reinforced slope were also noticeably smaller than those of the unreinforced slope. The strain response of element #3 on the boundary line between zone B and zone C showed similar behavior.

To examine the extent of the decrease due to piles in the two strain components, the following coefficients, the *shear effect coefficient* and *compression effect coefficient*, were defined:

$$\begin{cases} \text{shear effect coefficient} = \frac{\text{post−earthquake shear strain of unreinforced slope}}{\text{post−earthquake shear strain of reinforced slope}} \\ \text{compression effect coefficient} = \frac{\text{post−earthquake volumetric strain of unreinforced slope}}{\text{post−earthquake volumetric strain of reinforced slope}} \end{cases}$$

$$(2)$$

According to Eq. (2), the two coefficients reflect the extent of influence of the piles on shear deformation and compression deformation, respectively. It can be inferred that the larger the magnitude of each coefficient, the greater the effect of the piles on shear deformation and compression deformation. The shear effect coefficient and the compression effect coefficient of the four elements are outlined in Fig. 16. A demarcation line with an inclination of 45°, the angle of equivalence of the shear effect coefficient and the compression effect coefficient, is marked in the figure. It can be observed that the shear effect coefficient was nearly equal to the compression effect coefficient for element #1 on the inner side of the W-surface. The elements in the outer side of the W-surface (#2, #3, and #4) exhibited distinct features moving from the upper to the lower part of the slope. The W-surface was again justified as a valid way of demonstrating the influence of piles on the slope deformation during the strain analysis. In the upper part of the slope, near the slip surface of the unreinforced slope, the shear effect coefficient was greater than the compression effect coefficient of element #2, whereas the shear effect coefficient became smaller than the
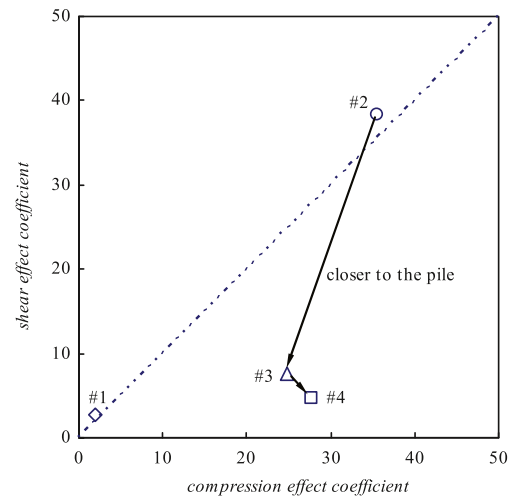
Fig. 16 Shear effect coefficient and compression effect coefficient of different elements (location indicated in Fig. 13) in the primary tests

compression effect coefficient in the lower part of the slope (i.e., for elements #3 and #4). Close examination of the shear effect coefficient and compression effect coefficient of the elements shows that the shear effect coefficient decreased as the element neared the piles. These findings indicate that the piles had a significant effect on the compression deformation of the slope in their vicinities, and this effect expanded upward within the slope on the outer side of the W-surface and arrested the slip surface that would have occurred in an unreinforced slope. Accordingly, the pile-decreased extent of the shear deformation was larger than that of the compression deformation at that point.

Conclusions and remarks

Centrifuge model tests were conducted to investigate the dynamic behavior of pile-reinforced slopes during an earthquake. The pile-reinforced behavior of the slope was focused mainly on the deformation analysis that was obtained over the entire slope through image-based measurement and compared to the behavior of an unreinforced slope. The main conclusions are as follows:

1. The piles significantly increased the stability level and reduced the deformation of a slope during an earthquake.
2. The bending moment of the piles exhibited nearly triangular distribution due to the earthquake. The bending moment decreased if the pile spacing or the slope gradient was reduced and increased if the pile location was moved from the lower part to the middle part of the slope.
3. The acceleration response of the slope increased with increasing elevation during the earthquake, which was affected by the pile layout and slope gradient.
4. The displacement exhibited an irreversible accumulation that was dependent on the input waves, slope gradient, and pile layout. The piles significantly affected the deformation of the slope in a certain area of the slope, and the boundary of this area was described using a continuous surface called the W-surface.

5. A strain analysis of the slope demonstrated that the piles had a significant effect on the deformation of the slope in their vicinities, and this effect expanded upward within the slope and arrested the possible slip surface that would have occurred in an unreinforced slope.
6. The features of input earthquake have a significant effect on the dynamic response of the reinforced slope.

The findings of this paper can enhance the understanding of pile reinforcement and help to set up an evaluation method of pile reinforcement effect of slopes that tend to slide.

References

Anbarasu K, Sengupta A, Gupta S (2010) Mechanism of activation of the Lanta Khola landslide in Sikkim Himalayas. Landslides 7(2):135–147

Ashford SA, Juirnarongrit T, Sugano T, Hamada M (2006) Soil–pile response to blast-induced lateral spreading.I: field test. J Geotech Geoenviron Eng 132(2):152–162

Ausilio E, Conte E, Dente G (2001) Stability analysis of slopes reinforced with piles. Comput Geotech 28(8):591–611

Brandenberg SJ, Boulanger RW, Kutter BL, Chang D (2005) Behavior of pile foundations in laterally spreading ground during centrifuge tests. J Geotech Geoenviron Eng 131(11):1378–1391

Cai F, Ugai K (2000) Numerical analysis of the stability of a slope reinforced with piles. Soils Found 40:73–84

El Sawwaf MA (2005) Strip footing behavior on pile and sheet pile-stabilized sand slope. J Geotech Geoenviron Eng 131(6):705–715

Gallagher RH (1974) Finite element analysis. Prentice-Hall, New Jersey

Huang RQ, Pei XJ, Fan XM, Zhang WF, Li SG, Li BL (2012) The characteristics and failure mechanism of the largest landslide triggered by the Wenchuan earthquake, May 12, 2008, China. Landslides 9(1):131–142

Imamura S, Hagiwara T, Tsukamoto Y, Ishihara K (2004) Response of pile groups against seismically induced lateral flow in centrifuge model tests. Soils Found 44(3):39–55

Ito T, Matsui T (1975) Methods to estimate lateral force acting on stabilizing piles. Soils Found 15(4):43–59

Jeong S, Kim B, Won J, Lee J (2003) Uncoupled analysis of stabilizing piles in weathered slopes. Comput Geotech 30(8):671–682

Kang GC, Song YS, Kim TH (2009) Behavior and stability of a large-scale cut slope considering reinforcement stages. Landslides 6(3):263–272

Martin GR, Chen CY (2005) Response of piles due to lateral slope movement Flac3D. Comput Struct 83(8–9):588–598

Mezazigh S, Levacher D (1998) Laterally loaded piles in sand: slope effect on p–y reaction curves. Can Geotech J 35(3):433–441

Poulos HG (1995) Design of reinforcing piles to increase slope stability. Can Geotech J 32(5):808–818

Rogers CDF, Glendinning S (1997) Improvement of clay soils in situ using lime piles in the UK. Eng Geol 47(3):243–257

Rosquoet F, Thorel L, Garnier J, Canepa Y (2007) Lateral cyclic loading of sand-installed piles. Soils Found 47(5):821–832

Smethurst JA, Powrie W (2007) Monitoring and analysis of the bending behaviour of discrete piles used to stabilise a railway embankment. Geotechnique 57(8):663–677

Take WA, Bolton MD, Wong PCP, Yeung FJ (2004) Evaluation of landslide triggering mechanisms in model fill slopes. Landslides 1(3):173–184

Take WA, Bolton MD (2001) The use of centrifuge modelling to investigate progressive failure of overconsolidated clay embankments. Workshop on Constitutive and Centrifuge Modelling: Two Extremes, Monte Verita, Switzerland

Thompson MJ, White DJ (2006) Design of slope reinforcement with small-diameter piles. ASCE Geotech Spec Publ 151:67–73

Thusyanthan NI, Madabhushi SPG, Singh S (2007) Tension in geomembranes on landfill slopes under static and earthquake loading—centrifuge study. Geotext Geomembr 25(2):78–95

Viswanadham BVS, Rajesh S (2009) Centrifuge model tests on clay based engineered barriers subjected to differential settlements. Appl Clay Sci 42(3–4):460–472

Wang LP, Zhang G, Zhang JM (2010) Nail reinforcement mechanism of cohesive soil slopes under earthquake conditions. Soils Found 50(4):459–469

Wang LP, Zhang G, Zhang JM (2011) Centrifuge model tests of geotextile-reinforced soil embankments during an earthquake. Geotext Geomembr 29(3):222–232

Yamagami T, Jiang JC, Ueno K (2000) Limit equilibrium stability analysis of slopes with stabilizing piles. ASCE Geotech Spec Publ 101:343–354

Zhang G, Hu Y, Zhang JM (2009) New image-analysis-based displacement-measurement system for centrifuge modeling tests. Measurement 42(1):87–96

Zhang G, Liang DF, Zhang JM (2006) Image analysis measurement of soil particle movement during a soil–structure interface test. Comput Geotech 33(4–5):248–259

Zhang LM, Ng CWW, Lee CJ (2004) Effects of slope and sleeving on the behavior of laterally loaded piles. Soils Found 44(4):99–108

Zornberg JG, Arriaga F (2003) Strain distribution within geosynthetic-reinforced slopes. J Geotech Geoenviron Eng 129(1):32–45

L. P. Wang · G. Zhang
State Key Laboratory of Hydroscience and Engineering,
Tsinghua University,
Beijing, China

G. Zhang (✉)
Institute of Geotechnical Engineering, Department of Hydraulic Engineering,
Tsinghua University,
Beijing, 100084, People's Republic of China
e-mail: zhangga@tsinghua.edu.cn